Journal of Electrical Engineering, Vol. 75, No. 5, 2024, pp. 351-362

sciendo

PAPERS

Improving primary frequency response in photovoltaic systems using hybrid inertia and intelligent control techniques

Chaouki Messasma[1], Seif Eddine Chouaba[1], Bilal Sari[1], Abdallah Barakat[2], Luis C. Félix-Herrán[3]

Low inertia poses a significant challenge to the widespread integration of photovoltaic (PV) systems into the grid, particularly affecting frequency stability. This paper addresses this challenge by proposing an advanced hybrid inertia (AHI) approach, characterized by the integration of real and virtual inertia, combined with the application of intelligent control techniques, to enhance the primary frequency response of a PV system. Internal inertia is provided by a synchronous generator (SG) acting as a compensator, while virtual inertia is generated through a real-time deloading strategy in the PV plant. The AHI is implemented on an isolated grid, utilizing various intelligent control techniques to improve frequency stability. The intelligent techniques employed include genetic algorithms (GA) and fuzzy logic controllers (FLC), which do not require mathematical modeling. This allows them to overcome the nonlinear dynamics of the PV plant and the uncertainties associated with climatic changes. These techniques are applied to the nonlinear components on the generator side, including the governor loop, DC-DC converter loop, and power reserve injection management loop. A frequency fluctuation scenario, induced by generating power perturbations in the proposed system, demonstrates and validates the improvement in frequency stability achieved by the HI and intelligent techniques. All tests are conducted using MATLAB Simulink. Various simulation results show a significant improvement in frequency stability through the incorporation of HI and intelligent control techniques.

Keywords: photovoltaics (PV), synchronous generator (SG), DC-DC boost converter, advanced hybrid inertia (AHI), virtual inertia control (VIC), genetic algorithm (GA), fuzzy logic controller (FLC)

1 Introduction

Photovoltaic (PV) systems are one of the most well-known renewable energy sources (RES) for replacing fossil fuels. However, the lack of internal inertia in PV structures is a significant barrier to integrating this type of energy source into the grid. Systems with considerable internal inertia demonstrate great frequency stability, and vice versa, which is consistent with the notion that internal inertia serves as a barrier against frequency droop, which is the first influence on the frequency response of any disturbance. As a result, in a system with high internal inertia, the natural resistance to changes in frequency is stronger, leading to smaller frequency deviations for a given disturbance. This means the system requires less frequency droop to maintain stability. Conversely, in a system with low internal inertia, frequency changes are more pronounced, necessitating a higher frequency droop to counteract these deviations and stabilize the system [1, 2].

Power systems manage frequency response through three control phases: primary, secondary, and tertiary. The primary control mechanisms consist of inertial response and droop response. The inertial response activates within 10 seconds of a frequency change, using the system's internal inertia to mitigate frequency deviations. The droop response then adjusts frequency by modulating reactive reserves for up to 20 seconds after the inertial response, aiding in further stabilization of the system. Automated generation control (AGC), a secondary control mechanism, takes 10 to 30 minutes to execute and restores the system frequency to its nominal value. Tertiary control, also known as reserve control, intervenes if the disturbance persists for more than 30 minutes [3].

The three main methods used to manage the scheduling of reserve services, primary, secondary, and tertiary, for maintaining frequency stability in the industry are sequential procurement, simultaneous scheduling of reserves, and integrated scheduling of energy and reserves [4].

The system's primary frequency response plays a critical role in stabilizing the system, primarily influenced by the total available inertia. Therefore, diminishing inertia, often through the substitution of synchronous generators with renewable energy sources

[1] Dosing Analysis and Characterization in High Resolution (DAC-HR) Laboratory, University of Setif1, Setif 19000 Algeria
[2] Electrical Energy Research Institute of Nantes-Atlantique (IREENA), Nantes Université, Nantes 44000 France
[3] Tecnologico de Monterrey, School of Engineering and Sciences Blvd, Hermosillo 83000 Mexico
e-mail:chaouki.messasma@univ-setif.dz

https://doi.org/10.2478/jee-2024-0043, Print (till 2015) ISSN 1335-3632, On-line ISSN 1339-309X

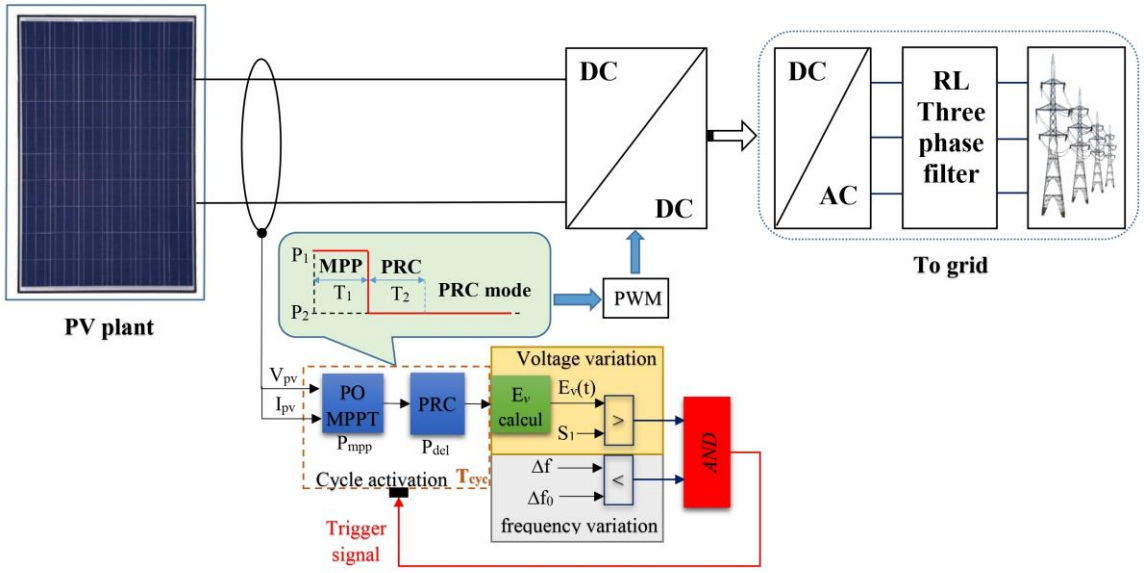

Fig. 1. Virtual inertia strategy

(RES), heightens the system's susceptibility to disturbances [5]. The inertia system is categorized into three types: hidden or real inertia, derived from the rotor component of synchronous generators, synthetic inertia, generated through various techniques to compensate for the lack of real inertia in RES-based systems, and emulated inertia, which mimics real inertias behavior through different methodologies in RES installations [6].

To maintain the smooth operation of solar power systems, control techniques, and auxiliary devices must be used to stabilize the frequency and improve the frequency response. The first method uses several auxiliary devices, such as batteries, flywheels, and various storage devices, to manage the frequency of the solar-powered system. The second method, which is based on deloading and inertia emulation techniques, is preferable because it does not require any additional equipment as the first one [6]. The methods utilized to integrate the PV system and enhance its frequency response, whether or not additional devices are used, are listed and described in depth in [6-8].

Deloading or power reduction approaches rely on operating the PV system outside of its maximum power point (MPP) to maintain the required power reserve. If there is any frequency change, the power reserve is injected as synthetic inertia. These deloading methods are utilized in two configurations: power reserve control (PRC), which generates a constant reserve with a variable working point, and constant power generation control (CPGC), which maintains a constant working point with a variable power reserve [9].

Another critical phase is integrating intelligent approaches such as fuzzy logic controllers (FLC), artificial neural networks (ANN), particle swarm optimization (PSO), genetic algorithms (GA), and others to maintain optimal frequency and inertia responses [10-13]. Roy et al [14] provide a review of inertia implementation in different simulation platforms using various intelligent control schemes to improve frequency and inertia responses.

The contribution of this work is improving the PV systems primary frequency response using Advanced Hybrid Inertia (AHI), which comprises hybrid inertia consisting of internal and virtual inertia coupled with intelligent control techniques. Internal inertia is generated without any energy creation by using a synchro-generator connected as a compensator. Virtual inertia is created through a deloading technique to maintain a power reserve, based on a cycle of two operating modes initiated by PV voltage fluctuation management. Various intelligent strategies were implemented in the integration of this hybrid inertia and compared to conventional methods, resulting in better participation and higher performance of the hybrid inertia.

The subsequent sections of the paper are structured as follows: Section 2 elaborates on the generation of hybrid inertia. Following this, Section 3 delves into primary frequency control, covering its two phases: droop control and virtual inertia control (VIC). In Section 4, the isolated grid configuration used in this study, along with its various control parts, is described. Section 5 outlines the intelligent control approaches employed in AHI, accompanied by the results of simulated tests conducted without hybrid inertia, with hybrid inertia (HI), and with AHI. The paper concludes with a summary of the work contributions and outlines future ambitions.

2 Hybrid inertia generation

In this study, hybrid inertia, consisting of two distinct types of inertia, is employed as previously presented and validated in [15]. The first type is synthetic or virtual inertia, generated by a PRC strategy installed in the PV plant. The second type incorporates the real inertia of the synchronous generator rotor.

The proposed HI approach is a real-time method that stands out from traditional inertia approaches due to its simplicity of implementation. Unlike conventional methods, it does not require modeling, complex mathematical calculations, assumptions, or prior knowledge of system parameters. Furthermore, it minimizes the use of sensors, particularly irradiation and temperature sensors, thereby avoiding the need for additional grid investments. These sensors not only increase grid costs and complexity but also introduce potential points of failure and errors, which can compromise the reliability and accuracy of the system. By bypassing these requirements, the HI approach offers a more robust and cost-effective solution [15,16].

The next subsections provide details about how to obtain these forms of inertia.

2.1 Virtual inertia

The lack of inertia that distinguishes PV systems from other sources of electricity means that they must supply a reserve of power to comply with frequency regulations [17]. Using an energy storage system and PRC strategies based on the deloading principle are the two main methods for achieving this goal. Furthermore, the requirement for any additional hardware as diverse energy storage devices employed in the first strategy would increase the grid cost and complexity; as a result, the second method, PRC strategy, is preferable.

A PRC approach, based on PV plant voltage variation detection, was applied in this research endeavor. This PRC approach comprises a cycle of two successive PV power converter operating modes, as shown in Fig. 1. The first one is the maximum power point tracking (MPPT) mode used to estimate and track the available PV power P_{mpp}. The MPPT mode accomplishes this task by using a simple perturb and observe (P&O) algorithm based on PV voltage and current measurements (V_{pv} and I_{pv}) [18]. The P_{mpp} value and its corresponding PV voltage V_{mpp} are memorized and transferred to the PRC mode once the MPPT mode is completed after the required time, which is set to T_1.

The second configuration, known as the PRC mode, starts when the MPPT phase ends. This mode is responsible for calculating the reference and new operating power P_{del} of the PV plant and doing so using the data received (P_{mpp} and V_{mpp}). This new reference power P_{del} is calculated as follows:

$$P_{del} = P_{pv} \cdot G_{del} \tag{1}$$

where G_{del} is the deloading gain specified by the grid operator.

During the PRC mode, the PV is brought to operate around the new operating point using a simple proportional integrator (PI) controller after calculating the P_{del} by using the G_{del} according to the desired power reserve. This mode, which lasts T_2, creates a power reserve P_{res} equal to the difference between the available PV power and the deloading power P_{res}=P_{mpp}−P_{del}.

The cycle begins after the PV plant is connected to the grid (the starting process) and lasts T_{cyc} seconds, which is equal to the sum of the durations of the two modes (T_1 + T_2). Following this period, the controller maintains PRC mode to produce the power reserve until the next cycle is initiated by the trigger signal. This trigger signal is responsible for monitoring the cycle activation based on variations in PV voltage through continuous PV voltage surveillance. Additionally, it detects any changes in the available power, which are primarily caused by weather fluctuations. The PV voltage surveillance is guaranteed by calculating the instantaneous relative error $E_v(t)$ of the observed V_{pv} as described in equation 2 and comparing it to a predefined threshold S_1. S_1 is set at 0.2% in this study and must be bigger than the voltage sensor error.

The $E_v(t)$ error is defined by the following equations:

$$E_v(t) = \frac{V_{del} - V_{pv}}{V_{max}} \tag{2}$$

V_{max} is the maximum voltage the voltage sensor can measure.

To allow the PV plant to participate in the frequency control loop, the trigger signal deactivates the cycle if the measured frequency deviation, Δf, exceeds the tolerable frequency deviation, Δf_0 set in this study to 49.95 Hz.

2.2 Internal inertia

Due to the increased adoption of renewable energy sources in electrical networks, certain synchro-nous generators (SG) are no longer in use. However, repurposing these SG to solely provide internal inertia incurs no additional costs. Real inertia is obtained by employing methods such as connecting the SG to the grid using a static frequency converter, without a prime mover, or utilizing techniques commonly employed in turbine pump hydro power stations. These SG are equipped with an excitation device that can function as a synchronous compensators or control reactive power

to zero. The nominal active power of the SG is minimized during electrical design, equivalent to the power required from the grid to operate the generator as a motor while recovering iron and friction losses. The real inertia supplied by the SG is represented by the inertia constant *H* or the moment of inertia of the rotor component. It is important to note that this paper focuses on the effect of SG on frequency regulation rather than the design aspects of the SG.

For a more detailed exploration and comprehensive understanding of hybrid inertia (HI) generation, including both virtual and real inertia, and its validation process, please refer to source [15]. This reference provides an extensive discussion of the mechanisms for generating synthetic or virtual inertia through a PRC strategy integrated into the PV plant. It also explains in detail the incorporation of real inertia derived from the rotor of a synchronous generator. The validation procedures outlined in source [15] offer a thorough examination and confirmation of the effectiveness and reliability of the proposed hybrid inertia approach.

3 Virtual inertia integration

Virtual inertial control (VIC), droop control, and combinations of the two approaches are the most popular ways to integrate PV systems with primary frequency control (PFC) [19-21]. The combined concept is employed in this work as fellow:

$$\Delta P_{PFC} = \Delta P_{droop} + \Delta P_{VIC} \tag{3}$$

Figure 2 depicts the integration of these two additional or extra amounts of power into the grid. These powers are injected according to frequency deviation; as the frequency decreases, it indicates that there is a greater demand for consumption power, in which case the extra power will be added. The increase in frequency indicates that there is more power than demand, the extra power will be subtracted from the PV plant's power. The two amounts are calculated in detail in the following:

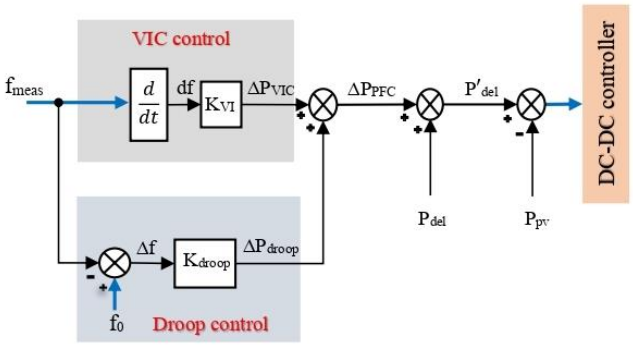

Fig. 2. VIC and droop control integration

3.1 Droop control

For conventional synchronous generators, a droop regulator is used to increase (or decrease) the power injected according to the change in the frequency system. The droop power used may be expressed as follows:

$$\Delta P_{droop} = K_{droop} \cdot \Delta f \tag{4}$$

where K_{droop} is the droop gain, tuned to integrate the entire power reserve when the frequency reaches its maximum nadir. Δf represents the frequency variation, calculated as

$$\Delta f = f_0 - f_{meas} \tag{5}$$

f_0 is the nominal frequency which is normally equivalent to 50 Hz or 60 Hz, and f_{meas} is the measured frequency.

3.2 Virtual inertia control (VIC)

Inertia determines the proportionate interaction between the active power and the frequency derivative or the rate of change of frequency (RoCoF). For PV systems to mimic inertia, the power provided by the PV panel to the grid must be proportional to the RoCoF, as:

$$\Delta P_{VIC} = 2H_{PV} \cdot \frac{df}{dt} = K_{VI} \cdot \frac{df}{dt} \tag{6}$$

H_{PV} is the PV plants equivalent virtual inertia constant. K_{VI} is the virtual inertia constant.

Implementing the proposed HI strategy in PV systems offers the significant advantage of avoiding additional grid investments, thereby potentially reducing overall project costs, as previously mentioned. However, achieving successful implementation requires careful consideration of several critical factors.

Firstly, ensuring accurate voltage monitoring is essential for effectively regulating the desired power reserve and its corresponding virtual inertia, and to prevent inaccuracies that could disrupt grid stability. This involves selecting precise and robust voltage sensors to accurately detect variations in climatic changes.

Managing dynamic responses effectively is equally crucial. Advanced control strategies are necessary to adjust power output in real-time, ensuring stability amidst the variability of PV outputs.

Optimizing deloading gain is vital to meet specific grid code requirements while maintaining the balance between the power injected from PV systems and the reserved power capacity.

This hybrid inertia is applied to a system consisting of a PV plant connected to an isolated grid that is simulated using the Matlab Simulink Package to demonstrate and present the effect of this inertia on enhancing frequency stability. The presentation of this system and its various control loops is detailed in the next section.

4 System and controller's illustration

Figure 3 illustrates the system utilized in this study, comprising an isolated grid modelled in Simulink software. The grid includes a large synchronous generator (main synchronous generator) with variable loads that can be abruptly altered using an additional load connected via a circuit breaker. These load fluctuations impact the grid frequency. Additionally, a second synchronous generator is linked to the grid and configured to provide only real inertia without active power generation, serving as compensation.

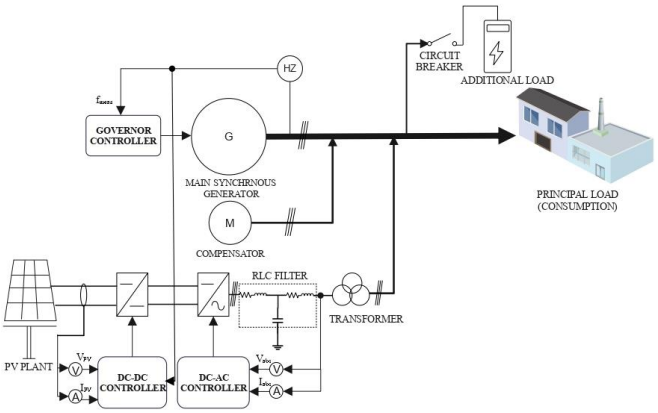

Fig. 3. Simulated system in Simulink

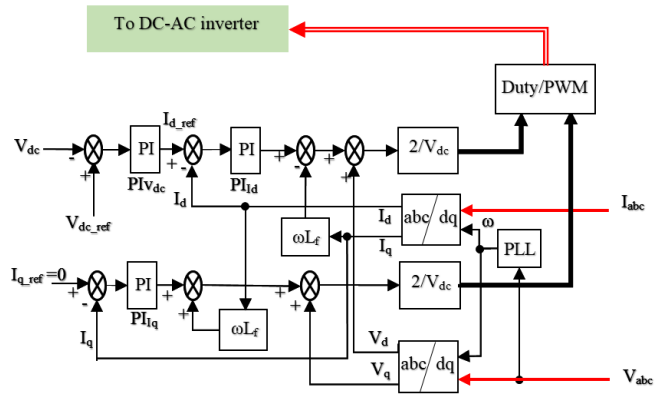

Fig. 4. DC-AC inverter control loop

The PV plant is integrated into the main grid through a double-stage system, as described in [22]. Generating 100.7 kW of power, the PV plant consists of 66 parallel strings, each comprising 5 Sun Power SPR-305E-WHTD modules in series. The management of the PV plant involves a DC-DC boost converter, controlled with the proposed real-time deloading strategy. In this configuration, the deloading gain is set to 0.8 to manage the PV at 80% of its P_{mpp} (maximum power point) while maintaining a power reserve of 20% (20 kW) to assist in frequency regulation. Subsequently, the plant is connected to a DC-AC inverter, controlled by a DQ current controller to ensure the transmission of the entire active power without any reactive power. The DC-AC inverter is controlled to maintain a constant DC voltage and zero reactive power, a common strategy with double-stage inverters, employing park transformation and decoupling between the d-axis and the q-axis, as explained in multiple papers [21-23], and illustrated in Fig. 4. All these components are equipped with RLC filters to mitigate harmonic effects before connecting to the grid via a transformer. For a detailed list of system components, please refer to Tab. 1.

The control of the proposed system comprises two main components: the generator side control, encompassing the main synchronous generator (SG) and the PV plant, which includes the governor controller and the DC-DC converter controller, and the grid side control, incorporating the DC-AC inverter controller. Subsequent sections will delve into the specific control loops utilized by each component.

4.1 Governor controller

Using a conventional PI, as shown in Fig. 5, this controller is in charge of modifying the speed of the main synchronous generator to regulate the power generated to meet demand with some power statism. The difference between the nominal and measured frequencies, as well as the rotor speed, constitute the controller's input and output, respectively. The proportional gain K_P and integrator gain K_I parameters of the PI controller are determined using both the trial-and-error approach and Matlab softwares tuning technique.

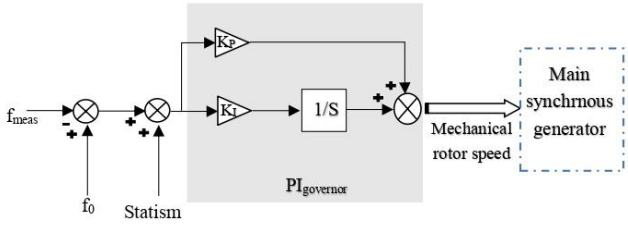

Fig. 5. Governor control loop

Table 1. System parameters

Symbol	Component	Value
Configuration parameters		
Grid	Main synchronous generator	302.1 kW
Compensator	Secondary synchronous generator	100.7 kW
PV	PV plant	100.7 kW
Consumption	Principal load	200 kW
Perturbation	Additional load	100 kW
Boost parameters		
L_{boost}	Boost converter inductance	0.54 mH
C_{pv}	PV plant capacitance	1400 µF
C_{dc}	DC link capacitance	6000 µF
V_{ref}	DC-link voltage reference	600 V
F_b	Converter switching frequency	5 kHz
K_{Pb}, K_{Ib}	Converter PI parameters	62, 8
Filter and grid parameters		
f_{inv}	Inverter switching frequency	25 kHz
f_0	Rated grid frequency	50 Hz
L_f	Filter inductance	0.85 mH
R_f	Filter resistance	1 m Ω
C_f	Filter capacitance	6000 µF
K_{Pdc}, K_{Idc}	DC voltage PI parameters	10, 0.1

4.2 DC-DC controller

As shown in Fig. 6, the boost converter has two operating modes: MPPT and delaoding mode. The signal command for the converter includes two positions, P_1 and P_2, with P_1 expanding to MPPT mode, which is the mode in which the P&O algorithm manages the converter. However, P_2 corresponds to the PRC mode, with the PI controller inputs P_{pv} and P'_{del} used to generate this mode control signal. The K_P and K_I parameters of this PI controller are determined also using both techniques: the trial-and-error approach and Matlab software tuning.

4.3 Power reserve (PR) controller

The primary frequency response encompasses both the hybrid inertia response, comprising real inertia and virtual inertia responses. The real or internal inertia response of a synchronous generator is an inherent and unalterable characteristic stemming from the physical properties of its rotating components, especially the rotor. It represents the natural kinetic energy stored in the generators mass and is not subject to external control. Instead, it spontaneously reacts to variations in power balance or disturbances within the system. The virtual inertia response is achieved through the management of the integration of the generated power reserve, as depicted in Fig. 2. This integration process, as previously described, involves two parts: the Droop control part and the VIC (Virtual Inertia Control) part.

4.4 Power reserve (PR) controller

The primary frequency response encompasses both the hybrid inertia response, comprising real inertia and virtual inertia responses. The real or internal inertia response of a synchronous generator is an inherent and unalterable characteristic stemming from the physical properties of its rotating components, especially the rotor. It represents the natural kinetic energy stored in the generators mass and is not subject to external control. Instead, it spontaneously reacts to variations in power balance or disturbances within the system. The virtual inertia response is achieved through the management of the integration of the generated power reserve, as depicted in Fig. 2. This integration process, as previously described, involves two parts: the Droop control part and the VIC part.

5 Intelligent techniques integration and simulation tests

5.1 Intelligent techniques integration

Classic control systems require deep knowledge of the controlled system as well as exact mathematical modeling. Due to the intermittent nature of RES, fluctuating system parameters, unpredictable fluctuations in load demand, and the presence of grid faults, standard control techniques may perform poorly, adapt inadequately, and become unstable under changing operating situations. These constraints have driven researchers to investigate and use more advanced and adaptive control strategies for highly nonlinear PV grid systems. Adaptive Neuro-Fuzzy Inference Systems (ANFIS), Fuzzy Logic (FL), Artificial Neural Networks (ANN), and evolutionary algorithms are some of the Artificial Intelligence (AI) techniques that are often employed. An intelligent control technique's main advantage is that it significantly boosts dynamic performance and enhances robustness to disturbances [26].

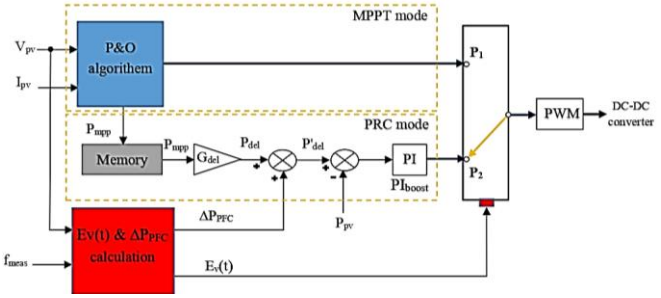

Fig. 6. DC-DC converter control loop

The described controller loops, including the governor, DC-DC boost, and PR (Power Reserve), were enhanced using advanced techniques to improve both high-frequency grid stability and overall hybrid inertia integration efficiency. Initially, the parameters of the different PI controllers, PI_{gov} and PI_{boost}, were fine-tuned using a genetic algorithm (GA) to optimize their performance. Subsequently, the PI_{boost} was replaced with a fuzzy logic controller to govern the converters operations, providing better adaptability to varying climatic conditions, temperature, and irradiation changes. Finally, a fuzzy controller was employed to manage PR integration, avoiding the need for exact parameter selection of conventional PR controller parameters K_{droop} and K_{VI}.

The next paragraphs describe the various controllers utilized, the simulation results for each of them, and a comparison of the controllers used to obtain the best possible one.

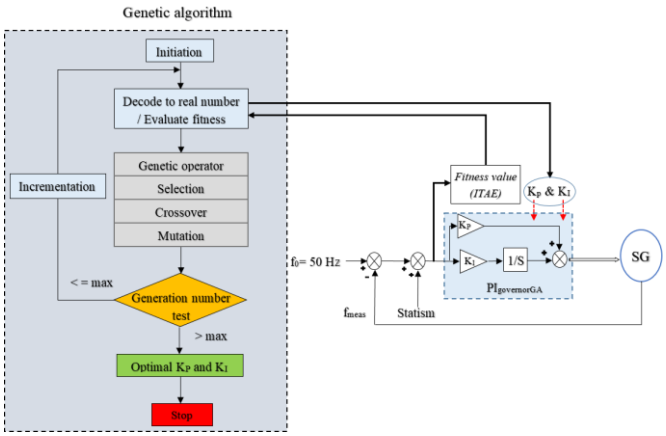

Fig. 7. PI_{govGA} structure

Governor controller update: The controller aims to adjust the grid rotor speed based on power demand. This controller is built on a PI controller, tuned using previously described techniques. It takes the difference between the measured frequency (f_{meas}) and the nominal frequency (f_0, set at 50 Hz) as inputs and outputs the reference mechanical rotor speed. In this phase, as shown in Fig. 7, the tuning process involves using a GA to determine the PI parameters (PI_{govGA}). The GA is widely used and applied in similar cases [27, 28]. The GA was configured with a population size of 50 individuals to ensure diverse exploration. A moderate mutation rate of 0.1 was chosen to balance exploration and maintain genetic diversity. To prevent premature convergence, the GA ran for 100 generations. A crossover rate of 0.8 was implemented to balance exploration and exploitation. Parent selection utilized tournament selection with a tournament size of 3, maintaining a balance between selection pressure and diversity. The GA aimed to minimize the Integral Time Multiplied Absolute Error (ITAE) value, described in Eqn. (7), serving as the fitness function. These parameter selections were the result of preliminary experiments, aiming to achieve a balance between computational efficiency and tuning effectiveness.

$$ITAE = \int_{t=0}^{t=final} |\Delta f| \cdot t \cdot dt \tag{7}$$

DC-DC controller update: The primary objective of this loop is to adjust the PV plant to the desired reference power in two situations: P_{mpp} represents the reference power in MPP mode, denoted as position P_1, and P'_{del} in PR mode, denoted as position P_2. This loop focuses on a PI controller tuned using a conventional technique, PI_{boost}, and then further tuned using GA for $PI_{boostGA}$. The GA is applied with the same parameters as previously detailed, as shown in Fig. 8.

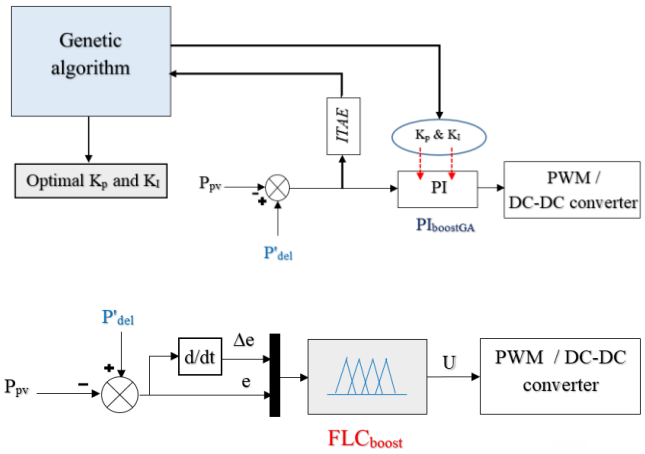

Fig. 8. $PI_{boostGA}$ tuning diagram and DC-DC control using FLC_{boost}

Integrating an FLC offers numerous advantages over traditional controllers like the PI controller, particularly in systems with nonlinearities or complex dynamics, such as renewable energy systems. Its adaptability allows it to adjust to changing operating conditions, making it suitable for systems with varying parameters or environments. The FLC simple rule base is intuitive and easier to develop compared to complex mathematical models, making it more accessible for implementation and tuning [29, 30]. In this context, as the second phase, the PI controller, PI_{boost}, of this loop is replaced by an FLC model as shown in Fig. 8. This FLC has two inputs: the error (e) between PV plant power and targeted power (P_{mpp} or P'_{del}) and its variation (Δe), and one output, which is the duty cycle of the DC-DC controller.

Table 2 outlines the FLC_{boost} guidelines that influence its decision-making process. These rules are developed based on numerous input variable combinations and implemented using the Mamdani approach, which leverages a series of fuzzy IF-THEN rules. Each rule describes the proper output for a given set of input variables. FLC_{boost} makes use of linguistic variables including negative big (NB), negative small (NS), zero (ZO), positive big (PB), and positive small (PS).

Figure 10 shows the input membership functions e and Δe and the output membership functions D of the FLC_{boost}.

Table 2. Fuzzy rules of FLC_{boost}

$\Delta e/e$	NB	NS	ZO	PS	PB
NB	NB	NB	NB	NS	ZO
NS	NB	NB	NS	ZO	PS
ZO	NB	NS	ZO	PS	PB
PS	NS	ZO	PS	PB	PB
PB	ZO	PS	PB	PB	PB

PR integration loop update: The goal of the PFC loop is to integrate the generated power reserve proportional to the frequency deviation. This loop is managed using a classical method, as described in Fig. 2 and Eqn. (3). This method focuses on the appropriate choice of its two parameters, K_P and K_I. These parameters determine the amount and speed of the extra power injected, which depend on various factors such as the PV plant power, the amount of power reserve, frequency droop, and nadir. This creates a nonlinear dynamic in the operation, necessitating adaptable parameter adjustments for K_P and K_I.

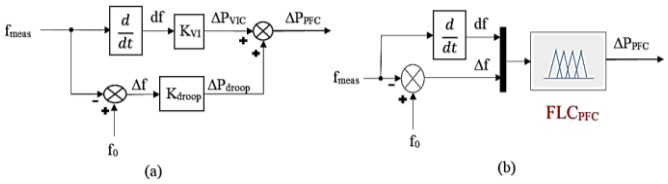

Fig. 9. PFC loop methods: (a) classical (b) FLC_{PFC}

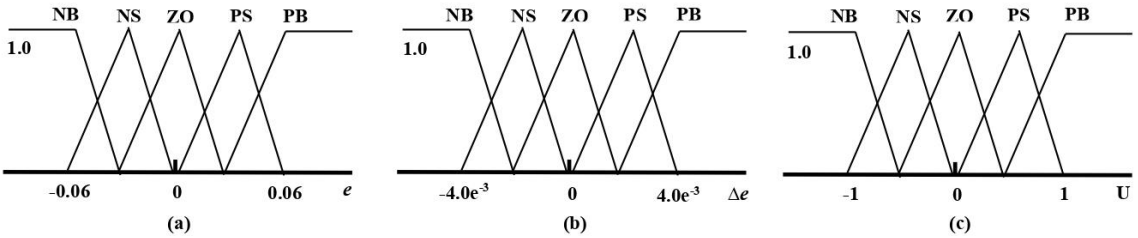

Fig. 10. FLC_{boost} membership functions input members: (a) error e, (b) change of error Δe. Output member (c) duty (U)

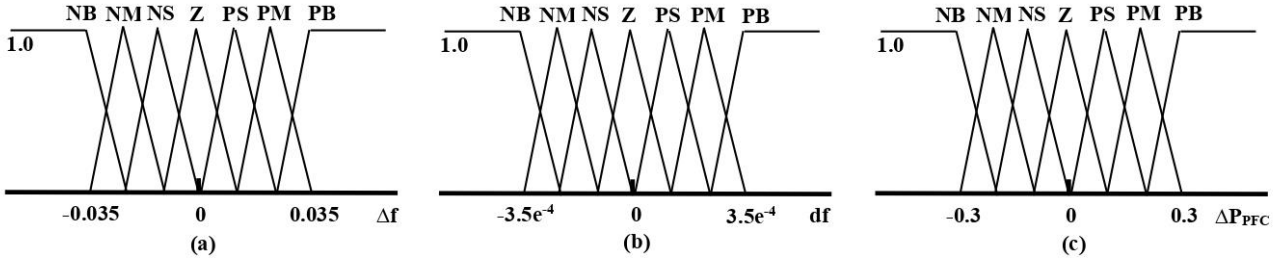

Fig. 11. FLC_{PFC} membership functions input members: (a) frequency variation Δf, (b) speed of frequency deviation (df). Output member: (c) injected power reserve ΔP_{PFC}

To address these challenges, an additional FLC is integrated to manage this task, as illustrated in Fig. 9. The frequency variation Δf and its rate df serve as inputs to the FLC model, with the output being the extra amount of power ΔP_{PFC}.

Table 3 outlines the PFC_{FLC} guidelines that influence its decision-making process. These rules are developed based on numerous input variable combinations and are implemented using the Mamdani approach, which leverages a series of fuzzy IF-THEN rules. Each rule describes the proper output for a given set of input variables. The PFC_{FLC} uses linguistic variables such as negative big (NB), negative medium (NM), negative small (NS), zero (ZO), positive big (PB), positive medium (PM), and positive small (PS).

Table 3. Fuzzy rules of FLC_{PFC}

d$f/\Delta f$	NB	NM	NS	ZO	PS	PM	PB
NB	NB	NM	NS	ZO	PS	PM	PB
NM	NB	NM	NS	ZO	PS	PM	PB
NS	NB	NM	NS	ZO	PS	PM	PB
ZO	NB	NM	NS	ZO	PS	PM	PB
PS	NB	NB	NB	ZO	PB	PB	PB
PM	NB	NB	NB	ZO	PB	PB	PB
PB	NB	NB	NB	ZO	PB	PB	PB

Figure 11 shows the input membership functions Δf and df and the output membership functions ΔP_{PFC} of the PFC_{FLC}.

5.2 Tests and discussion

To demonstrate the superiority of the proposed system using conventional configurations and after applying various intelligent techniques, two main scenarios were applied for different configurations using different developed controllers: PI_{gov}, PI_{govGA}, PI_{boost}, $PI_{boostGA}$, FLC_{boost}, and FLC_{PFC}. These con-figurations were tested in various combinations.

In the first scenario, different configurations were subjected to power disturbances to emulate frequency fluctuations. The power imbalance was simulated by adding and removing an extra load via a circuit breaker at t = 80 s and t = 140 s, respectively. Throughout all tests, the irradiation was set to 1000 W/m^2, the temperature was maintained at 25 °C, and the deloading gain was set to 0.8.

In the second scenario, the system experienced frequency fluctuations in two distinct situations. The first situation operated without frequency regulation service, meaning no AHI integration. This setup highlighted the performance of each controller in an environment without additional frequency support mechanisms. The second situation enabled frequency regulation by integrating HI and AHI, providing additional support to maintain grid stability. This configuration evaluated how each controller benefited from or interacted with the frequency regulation service. These tests highlighted the performance, stability, and adaptability of each configuration in managing frequency fluctuations.

Table 4 summarizes each controller and the tests they underwent.

Table 4. Summary of controllers and tests

Controller/Test	Frequency perturbation	AHI integration
Governor	√	X
DC-DC boost	√	√
PR integration	√	√

Figure 12 depicts the simulation results of the first test, which involves subjecting both PI_{gov} and PI_{govGA} configurations to the described frequency perturbation scenario. The grid frequency and PV plant power illustrated in this figure show that the grid frequency reaches a nadir of 49.799 Hz using PI_{gov} and a nadir of 49.923 Hz using PI_{govGA}. This demonstrates the effectiveness of PI_{govGA} by improving the frequency nadir by 0.124 Hz and reducing the frequency droop from 0.201 Hz (0.402%) to 0.077 Hz (0.154%). The same figure shows the PV plant power output of 80 (kW) while maintaining a power reserve of 20 kW, which is 20% of the maximum power 100 kW, without any PR integration as previously configured. Additionally, the real or internal inertia is not integrated, resulting in the absence of frequency regulation services in this configuration.

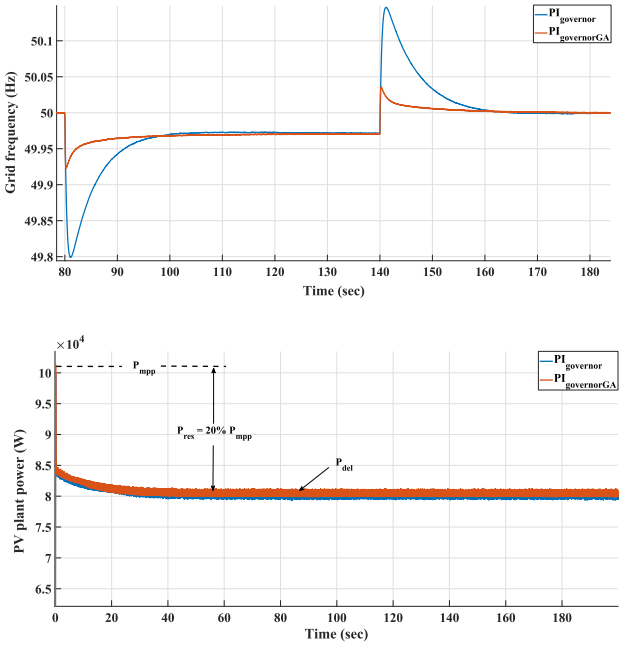

Fig. 12. Grid frequency and PV plant power using PI_{gov} and PI_{govGA}

From the first test, PI_{govGA} demonstrates its superiority over the conventional one. For this reason, it will be kept as the governor controller in the subsequent tests.

Figures 13 and 14, along with Table 5, provide detailed insights into the grid characteristics, grid frequency, PV plant power, and compensator active power results of tests using different configuration combinations. Initially, the benefits of employing conventional HI are evident, showcasing a reduction in the frequency nadir from 49.799 Hz to 49.861 Hz, a decrease in frequency droop from 0.201 Hz (0.402%) to 0.139 Hz (0.278%), but an increase in response time from 14.10 s to 14.85 s in load impact. This effect is also observed in load shedding, with a reduction in the frequency nadir from 50.146 Hz to 50.085 Hz, a decrease in frequency droop from 0.146 Hz (0.293%) to 0.085 Hz (0.175%), and decreases in nadir time from 141.16 s to 140.9 s, but an increase in response time from 16.44 s to 23.10 s.

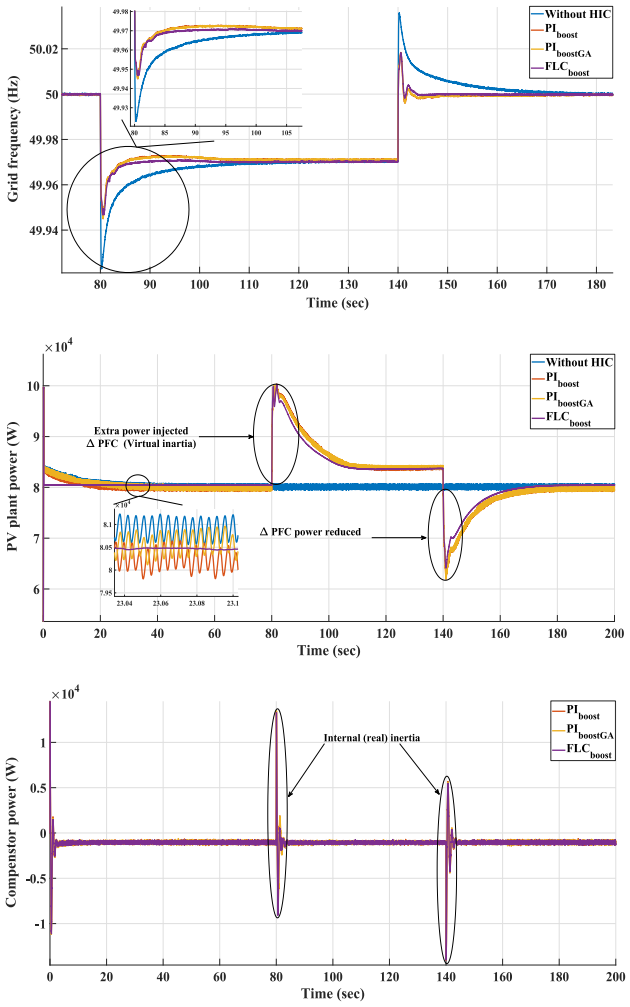

Fig. 13. Grid frequency, PV plant power and compensator power using PI_{boost}, $PI_{boostGA}$ and FLC_{boost}

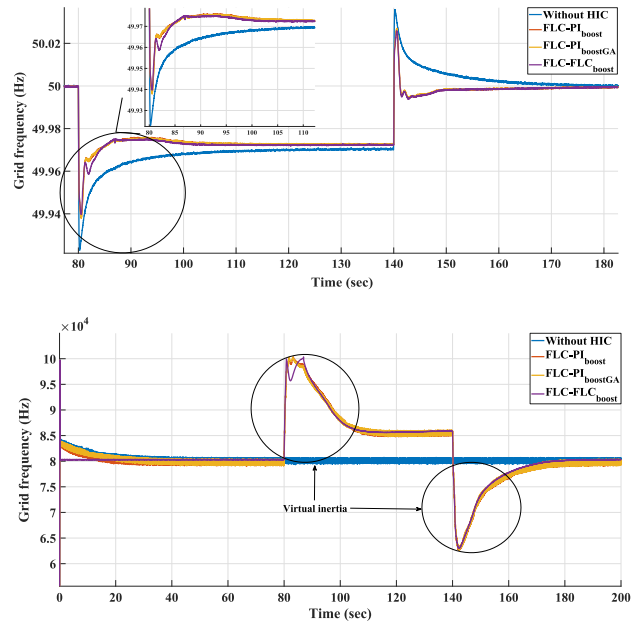

Fig. 14. Grid frequency and PV plant power using FLC-PI_{boost} , FLC-$PI_{boostGA}$ and FLC-FLC_{boost}.

Subsequently, the efficacy of intelligent control approaches is illustrated by utilizing the AHI, which includes PI_{govGA} as the governor controller, FLC_{boost} as the DC-DC boost controller, and an FLC model in PFC integration (FLC_{PFC}). This configuration results in a further significant reduction in frequency nadir to 49.940 Hz, a reduction of frequency droop to 0.06 Hz (0.120%), a decrease in nadir time to 80.53 s, and a significant reduction in response time to 4.47 s in load impact. Moreover, better results are achieved in load shedding, with a reduction in frequency nadir to 50.026 Hz, a reduction of frequency droop to 0.026 Hz (0.05%), a decrease in nadir time to 140.059 s, and a significant reduction in response time to 0.59 s.

Figure 15 illustrates the outcomes obtained with AHI compared to conventional HI and without HI incorporation. This visualization highlights the significant contributions made by AHI in both disturbance power scenarios, as well as improvements in the DC-DC converter's response time.

Furthermore, it ensures excellent response quality devoid of oscillations and maintains high system stability. As previously discussed, internal inertia is a natural reaction and is not linked to any controller. This justifies that the compensator does not generate any active power until a frequency perturbation appears. At t = 80 s, the compensator provides a constant quantity of power as internal inertia, injecting 12.98 kW proportional to the frequency deviation direction under all configurations, as shown in Fig. 13.

The illustrated results of tests in various figures and Tab. 5 underscore the substantial improvement afforded by a real-time deloading technique integrated with diverse intelligent techniques. This enhancement is evidenced by the notable reduction in frequency nadir and response time, both of which play critical roles in bolstering grid frequency stability. The decrease in frequency nadir reflects the system's enhanced ability to manage sudden disturbances and fluctuations, thereby ensuring that grid frequency remains within acceptable limits. Moreover, the observed reduction in response time signifies a more agile and responsive system, capable of swiftly adapting to changes in operating conditions and mitigating the adverse effects of frequency deviations. Collectively, these findings highlight the pivotal role of intelligent techniques in fortifying the stability and reliability of power systems, offering operators a robust framework to navigate the complexities of modern grid operations and enhance overall system performance.

Table 5. Global test results

Controller employed			f_{nadir} (Hz)	Δf (Hz & %)	T_{nadir} (s)	$T_{response}$ (s)
Governor	Boost	HIC				
LOAD IMPACT						
PI_{gov}	PI_{boost}	Without	49.799	0.201 (0.402%)	81.10	14.10
PI_{govGA}	PI_{boost}	without	49.923	0.077 (0.154%)	80.23	15.27
PI_{gov}	PI_{boost}	classical PFC	49.861	0.139 (0.278%)	81.15	14.85
PI_{govGA}	PI_{boost}	classical PFC	49.945	0.055(0.110%)	80.54	3.26
PI_{govGA}	$PI_{boostGA}$	classical PFC	49.945	0.055(0.110%)	80.54	3.26
PI_{govGA}	FLC_{boost}	classical PFC	49.947	0.053 (0.106%)	80.51	3.29
PI_{govGA}	PI_{boost}	FLC_{PFC}	49.938	0.062 (0.123%)	80.54	5.03
PI_{govGA}	$PI_{boostGA}$	FLC_{PFC}	49.938	0.062 (0.124%)	80.56	5.03
PI_{govGA}	FLC_{boost}	FLC_{PFC}	49.940	0.060 (0.120%)	80.53	4.47
LOAD SHEDDING						
PI_{gov}	PI_{boost}	Without	50.146	0.146 (0.293%)	141.16	16.44
PI_{govGA}	PI_{boost}	without	50.035	0.035 (0.071%)	140.25	19.75
PI_{gov}	PI_{boost}	classical PFC	50.085	0.085 (0.175%)	140.90	23.10
PI_{govGA}	PI_{boost}	classical PFC	50.183	0.183 (0.366%)	140.59	0.29
PI_{govGA}	$PI_{boostGA}$	classical PFC	50.184	0.184 (0.368%)	140.55	0.34
PI_{govGA}	FLC_{boost}	classical PFC	50.183	0.183 (0.366%)	140.56	0.35
PI_{govGA}	PI_{boost}	FLC_{PFC}	50.027	0.027 (0.053%)	140.59	0.62
PI_{govGA}	$PI_{boostGA}$	FLC_{PFC}	50.027	0.027 (0.053%)	140.58	0.62
PI_{govGA}	FLC_{boost}	FLC_{PFC}	50.026	0.026 (0.051%)	140.59	0.59

Here, $f_{variation}$ is the minimum or highest frequency value registered when frequency deviation appears, $T_{variation}$ is the time of $f_{variation}$ and $T_{response}$ is the duration required to restore the frequency from the $f_{variation}$ to 95% of its final value.

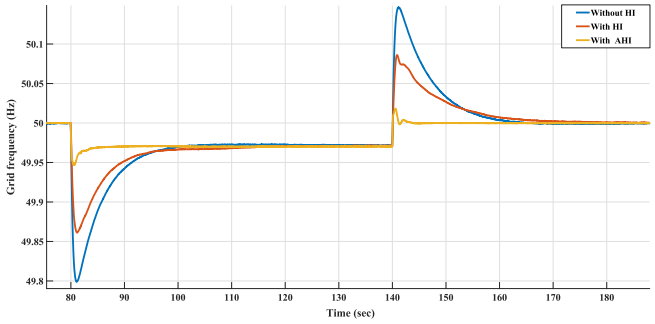

Fig. 15. Grid frequency: without HI, with HI, and with AHI

6 Conclusion

This paper introduces a real-time advanced hybrid inertia technique designed to enhance the frequency stability of grids integrated with photovoltaic systems. The proposed approach involves a hybrid inertia that combines internal and virtual inertia, offering a straightforward implementation without the need for complex mathematical models, assumptions, or additional hardware investments. This HI helps to improve frequency stability and can be easily adapted to various configurations. Integrating this HI with advanced intelligent methods, resulting in AHI, significantly enhances grid performance by reducing frequency nadir, droop, and response time, while simultaneously increasing stability and minimizing oscillations. To ensure robustness under diverse climatic conditions, the adoption of robust control methodologies is crucial. These strategies enable systems to withstand weather-related uncertainties and disturbances, thereby enhancing their reliability and performance across different environments.

References

[1] O. Gandhi, D. S. Kumar, D. Rodriguez-Gallegos and D. Srinivasan, "Review of power system impacts at high PV penetration Part I: Factors limiting PV penetration," *Solar Energy*, 210, 181-201, 2020. doi: 10.1016/j.solener.2020.06.097.

[2] D. S. Kumar, O. Gandhi, C. D. Rodriguez-Gallegos and D. Srinivasan, *"Review of power system impacts at high PV penetration Part II: Potential solutions and the way forward," Solar Energy*, 210, 202-221, 2020. doi: 10.1016/j.solener.2020.08.047.

[3] M. N. H. Shazon and A. Jawad, "Frequency control challenges and potential countermeasures in future low-inertia power systems: A review," *Energy Reports*, 8, 6191-6219, 2022. doi:10.1016/j.egyr.2022.04.063

[4] F. D. Galiana, F. Bouffard, J. M. Arroyo and J. F. Restrepo, "Scheduling and pricing of coupled energy and primary, secondary, and tertiary reserves," *Proceedings of the IEEE*, 93(11), 1970-1983, 2005. doi: 10.1109/JPROC.2005.857492

[5] M. Alam, T. A. Chowdhury, A. Dhar, F. S. Al-Ismail, M. S. H. Choudhury, M. Shafiullah and S. M. Rahman, "Solar and Wind Energy Integrated System Frequency Control: A Critical Review on Recent Developments," *Energies*, 16(2), 812, 2023. doi: 10.3390/en16020812

[6] S. A. Hasen, Ş. Sonmez and S. Ayasun, "Enhancement of stability delay margins by virtual inertia control for microgrids with time delay," *Turkish Journal of Electrical Engineering and Computer Sciences*, 30(6), 2221-2236, 2022. doi: 10.55730/1300-0632.3935

[7] M. S. Alam, F. S. Al-Ismail, A. Salem and A. Abido, "High-level penetration of renewable energy sources into grid utility: Challenges and solutions," *IEEE Access*, 8, 190277-190299, 2020. doi: 10.1109/ACCESS.2020.3031481

[8] U. Akram, M. Nadarajah, R. Shah and F. Milano, "A review of rapid responsive energy storage technologies for frequency regulation in modern power systems," *Renewable and Sustainable Energy Reviews*, 120, 109626, 2020. doi:10.1016/j.rser.2019.109626

[9] M. Dreidy, H. Mokhlis and S. Mekhilef, "Inertia response and frequency control techniques for renewable energy sources: A review," *Renewable and sustainable energy reviews*, 69, 144-155, 2017. doi: 10.1016/j.rser.2016.11.170

[10] A. Mahrouch and M. Ouassaid, "Primary Frequency Regulation Based on Deloaded Control, ANN, and 3D-Fuzzy Logic Controller for Hybrid Autonomous Microgrid," *Technology and Economics of Smart Grids and Sustainable Energy*, 7(1), 1-12, 2022. doi: 10.1007/s40866-022-00125-2

[11] M. Ali, H. Kotb, M. K. AboRas and H. N. Abbasy, "Frequency regulation of hybrid multiarea power system using wild horse optimizer based new combined Fuzzy Fractional-Order PI and TID controllers," *Alexandria Engineering Journal*, 61(12), 12187-12210, 2022. doi:10.1016/j.aej.2022.06.008

[12] M. Moeti and M. Asadi, "Robust model reference adaptive PI controller-based sliding mode control for the three-phase grid-connected photovoltaic inverter," *Turkish Journal of Electrical Engineering and Computer Sciences*, 29(1), 257-275, 2021. doi: 10.3906/elk-2004-145

[13] A. Abazari, M. Babaei, S. M. Muyeen and I. Kamwa, "Learning adaptive fuzzy droop of PV contribution to frequency excursion of hybrid micro-grid during parameters uncertainties," *International Journal of Electrical Power & Energy Systems*, 123, 106305, 2020. doi: 10.1016/j.ijepes.2020.106305

[14] N. K. Roy, S. Islam, A. K. Podder, T. K. Roy and S. M. Muyeen, "Virtual Inertia Support in Power Systems for High Penetration of Renewables‐ Overview of Categorization, Comparison, and Evaluation of Control Techniques," *IEEE Access*, 2022. doi: 10.1109/ACCESS.2022.3228204

[15] C. Messasma, A. Barakat, S. eddine Chouaba and B. Sari, "PV system frequency regulation employing a new power reserve control approach and a hybrid inertial response," *Electric Power Systems Research*, 223, 109556, 2023. doi:10.1016/j.epsr.2023.109556

[16] C. Messasma, S. E. Chouaba, B. Sari and A. Barakat, "Power reserve control (PRC) of PV systems techniques overview," *In 2022 19th International Multi-Conference on Systems, Signals & Devices (SSD)* (pp. 1466-1470). IEEE, 2022, May. doi: 10.1109/SSD54932.2022.9955657

[17] Y. Zhang, X. Liu, Y. Wu, S. E. Wang, Y. Wang, Z. Tang and J. Hao, "Analysis of Inertia Mechanism of Grid-tied Photovoltaic Power Generation System with Virtual Inertia Control," *In 2019 4th IEEE Workshop on the Electronic Grid (eGRID)* (pp. 1-6). IEEE, 2019, November. doi: 10.1109/eGRID48402.2019.9092695

[18] R. Ayop and C. W. Tan, "A comprehensive review on photovoltaic emulator," *Renewable and Sustainable Energy Reviews*, 80, 430-452, (2017). doi: 10.1016/j.rser.2017.05.217

[19] J. G. Ramos and R. E. Aráujo, "Virtual inertia and droop control using DC-link in a two-stage PV inverter," *In 2020 IEEE 14th International Conference on Compatibility, Power Electronics and Power Engineering (CPE-POWERENG)* (Vol. 1, pp. 55-60). IEEE, 2020, July. doi:10.1109/CPEPOWERENG48600.2020.9161610

[20] Q. Peng, Y. Yang, T. Liu and F. Blaabjerg, "Coordination of virtual inertia control and frequency damping in PV systems for optimal frequency support," *CPSS Transactions on Power Electronics and Applications*, 5(4), 305-316, 2020. doi: 10.24295/CPSSTPEA.2020.00025

[21] R. Rajan and F. M. Fernandez, "Power control strategy of photovoltaic plants for frequency regulation in a hybrid power system," *International journal of electrical power & energy systems*, 110, 171-183, 2019. doi: 10.1016/j.ijepes.2019.03.009

[22] V. Kumar and M. Singh, "Reactive power compensation using derated power generation mode of modified P&O algorithm in a grid-interfaced PV system," *Renewable Energy*, 178, 108-117, 2021.

[23] S. M. Nosratabadi and E. Gholipour, "Power system harmonic reduction and voltage control using DFIG converters as an active filter," *Turkish Journal of Electrical Engineering and Computer Sciences*, 24(4), 3105-3122, 2016. doi:10.1016/j.renene.2021.06.035

[24] H. Athari, M. Niroomand and M. Ataei, "Review and classification of control systems in grid-tied inverters," *Renewable and Sustainable Energy Reviews*, 72, 1167-1176, 2017. doi:10.1016/j.rser.2016.10.030

[25] S. Sezen, A. Aktaş, M. Uçar and E. Özdemir, "Design and operation of a multifunction photovoltaic power system with shunt active filtering using a single-stage three-phase multilevel inverter," *Turkish Journal of Electrical Engineering and Computer Sciences*, 25(2), 1412-1425, 2017. doi: 10.3906/elk-1602-381

[26] N. Chettibi and A. Mellit, "Intelligent control strategy for a grid-connected PV/SOFC/BESS energy generation system," *Energy*, 147, 239-262, 2018. doi: 10.1016/j.energy.2018.01.030

[27] B. Nagarani and J. Nesamony, "Performance enhancement of photovoltaic system using genetic algorithm-based maximum power point tracking," *Turkish Journal of Electrical Engineering and Computer Sciences*, 27(4), 3015-3025, 2019. doi:10.3906/elk-1801-189

[28] M. S. Saad, H. Jamaluddin and I. Z. M. Darus, "Implementation of PID controller tuning using differential evolution and genetic algorithms," *International Journal of Innovative Computing, Information, and Control*, 8(11), 7761-7779, 2012.

[29] M. S. Omar, A. El-Deib, A. L. El Shafei and M. E. Abdallah, "Comparative study between PI and fuzzy-logic controllers for three-phase grid-connected photovoltaic systems," *In 2016 Eighteenth International Middle East Power Systems Conference (MEPCON)* (pp. 380-386). IEEE, 2016, December. doi: 10.1109/MEPCON.2016.7836919

[30] R. Rajan and F. M. Fernandez, "Fuzzy-based control of the grid-connected photovoltaic system for enhancing system inertial response," *In 2018 53rd International Universities Power Engineering Conference (UPEC)* (pp. 1-6). IEEE, 2018, September. doi: 10.1109/UPEC.2018.8542008

Received 7 June 2024